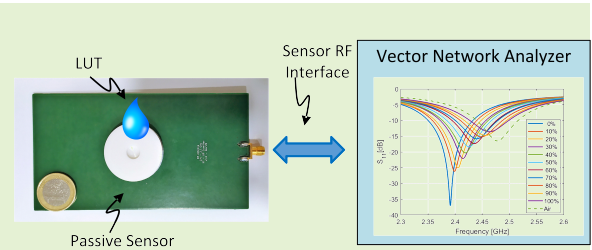


A novel dielectric resonator-based passive sensor for drop-volume binary mixtures classification

Mahdieh Gholami Mayani, *Student Member, IEEE*, Francisco Javier Herraiz-Martínez, *Member, IEEE*, Javier Matanza Domingo, Romano Giannetti, *Senior Member, IEEE* and Carlos Rodríguez-Morcillo García

Abstract—In this study, the authors present a dielectric-resonator-based sensor to characterize liquids. The sensor is based on a dielectric resonator (DR) fed by a slot-coupling mechanism in the ground plane of a microstrip transmission line (TL). The obtained device is a fully passive sensor that a radiofrequency (RF) signal can interrogate. A small hole was drilled on the DR surface to allocate a drop of the liquid under test (LUT); as a consequence, the resonant frequency of the sensor will depend on the electromagnetic characteristics of the LUT. The device is modeled both with an equivalent circuit model and through an electromagnetic modal analysis. The cavity perturbation technique is used to study the impact of the LUT on the resonant frequency and modal distribution; full-wave simulations corroborate the theoretical results. Finally, a prototype of the proposed sensor tuned to work in the 2.45 GHz band has been designed, manufactured, and measured. The device is cost-effective given the small size and practical to use, thanks to the minimal volume of the pool, which calls for quantities of LUT in the order of $0.13 \mu\text{l}$. The prototype has been tested with an ethanol-water solution set. The experimental results match well with simulations and show good repeatability. The sensitivity of the prototype resulted in being 718 kHz per percentage of ethanol in water.

Index Terms—Dielectric Resonator (DR), Electromagnetic sensor, ISM band, Liquid sensor.



I. INTRODUCTION

CHEMICAL substances dissolved in different solvents such as water, blood and urine can modify the electromagnetic properties of those solutions. The main changes in dielectric properties correspond to the permittivity and loss tangent of the solvent [1]. Since each material has a distinct natural property, therefore, characterization of chemical solutions can be conducted by means of different detecting approaches sensitive to the loss factor and permittivity specifications.

Microwave techniques can be effectively applied as a rigorous solution to characterize and classify materials and solutions. For example, these techniques were recently proposed to indicate the imbalances in the concentration of certain electrolytes in blood or urine such as sodium chloride (NaCl) and glucose, in comparison with typical level existing in healthy samples [2]. Sensors working in the radio frequency (RF) and the microwave regime are one of the best techniques for sensing, characterize and classify materials due to their versatility, low-power consumption, easy fabrication and cost effectiveness [3]–[5]. Regarding the power consumption, most

of them are fully passive, which means that no batteries are needed.

To discriminate small variations of the material of interest, it is critically needed to have a high resolution sensors. In order to achieve this goal, high quality and low loss factors are prerequisites for sensor operation. To this end, several planar sensing structures have been proposed [4], [6]–[12]. Among them, frequency-domain-based sensors are the predominant category. Their working principle is based on the shift in their resonant frequency by changing the capacitance of the original prototype. This is usually obtained by placing the sample under test over the sensitive area of the sensor [13].

In frequency-domain category, many structures have been applied to characterize liquid materials and solutions. In many cases, this type of sensors such as submersible ones, require a big amount of fluid material as they should be merged in the solution [10], [12]. In some applications such as biological testing, the necessity to afford this volume of material is squandering. To tackle this problem, microfluidic sensors are proposed. Microfluidic sensors with low volumes and high accuracy are promising as they can be developed in chip-based compact configurations [4], [14]. Compared to the submersible sensors, microfluidic sensors suffer from more complexity and cost as a microfluidic channel is located on the most sensitive area of the resonators. A comprehensive review by the same authors has been recently published in IEEE TIM

M. Gholami Mayani, F. J. Herraiz-Martínez, J. Matanza, R. Giannetti and C. Rodríguez-Morcillo García are with the Instituto de Investigación Tecnológica (IIT), Comillas Universidad Pontificia, Calle de Santa Cruz de Marcenado, 26 - 28015 Madrid, Spain

[13]. Although the aforementioned sensors demonstrate an acceptable sensitivity and dynamic range, the detection of small variations in permittivity of samples is limited by the resonant elements; especially in some structures, the saturation behavior emerges after a specific level. Indeed, there are multiple capacitors in the planar resonators whereas one of them is the most sensitive capacitance which can be incorporated as sensing element. As a result, the sensitivity is limited in the planar resonator-based sensors. In addition, by decreasing the operation frequency, the size of structures gets larger, considered as a serious concern. In order to increase the sensitivity, several attempts have been made. For instance, substrate-integrated waveguide (SIW) technology maintaining the functionality of conventional waveguides benefits from high Q-factor and high power handling capability [15], [16]. However, they suffer from complexity in fabrication. The array configuration is another strategy for increasing the sensitivity and Q-factor. This type of sensors with high performance suffer from large surface area and hence, the need for a big amount of sample [17]. Besides, capacitive sensors with the advantage of contactless drop characterization have been studied in [18], [19]. The typical operation principle is based upon cylindrical conducting electrodes wherein minimal insulating gaps are placed between the electrodes to isolate them from the neighboring electrodes. The change in the cross capacitance is evaluated when a droplet is placed in the region within the electrodes. This capacitance variation, a consequence of the dielectric permittivity change, is used to discriminate the materials under test. The sensor in the time-domain approach shows a good functionality for several volume variations for oil, water, ethanol and acetone, as well as dynamic capacitive response corresponding to different salt concentrations.

Dielectric Resonators (DR) are made up of ceramic materials and some commercial polymers. Their high dielectric permittivity leading to high stored energy within the DR cavity and low dissipation (loss) factor makes these resonators a promising alternative. These resonant elements have been applied to oscillators, filters and antennas for decades [20]–[23]. Recently, DR with high efficiency, compact size and cost-effectiveness have attracted the researcher's consideration in sensing applications [22], [24]–[28]. The size of the DR inversely depends upon the relative permittivity of its constitutive material. The higher the relative permittivity of the constitutive material of DR, the lower the size of the DR. Contrariwise, the impedance matching and bandwidth are reduced by increasing the permittivity constant [29] resulting in having a quite narrow bandwidth. This narrow bandwidth is undesired in most applications, but this may be beneficial in some applications such as sensors. As explained before, frequency-domain-based sensors are favored to work with narrow bandwidths and high Q factor values.

In this paper a novel DR sensor for liquid characterization is proposed. This is based on a cylindrical DR working in the 2.45-GHz band excited by slot feeding. This feeding technique is based on a microstrip transmission line (TL) with a slot in its ground plane. The DR is placed over the ground plane and coupled to the TL through the slot. By creating a small pool on top of the DR surface, the liquid under test (LUT)

can be placed and sensed as a slight change in the resonant frequency is induced. This frequency change depends on the dielectric characteristics of the LUT, allowing an accurate determination of solvent concentrations. The main advantages of the proposed DR-based sensor in comparison with the planar resonator-based sensors are their great Q-factor, high resolution, independency to the temperature and high accuracy. These beneficial aspects make these sensor suitable to characterize low volumes of liquid samples and solutions. Moreover, the need of low volumes of LUT represents a benefit compared to submersible sensors which makes this novel sensor suitable for measuring biological samples in the future. On the other hand, its robustness, simplicity in fabrication and low cost over other more complex approaches such as microfluidic, SIW-based and array-based make the proposed DR-based sensor a good candidate for sensing liquids in mass applications. To the best of our knowledge, it is the first time that a DR-based sensor, at the low-GHz frequency range, is analytically and experimentally studied for characterizing low-volume liquid samples.

This paper is organized as follow: In section II, the geometry of DR-based sensor in addition to its sensing principle are explained. In section III, the modal analysis of the proposed sensor is studied and the perturbation method is applied to analyze the effect of a sample on the resonant modes. A study of the dielectric characterization of the ethanol-water solutions used to test the sensor is presented in Section IV. Since, ethanol-water mixture is a classical choice to test sensors, enabling us to compare the proposed structure easily with existing literature [30] and [31]. In section V the sensor is simulated and experimentally tested. The results are verified with different ethanol-water solutions and the main characteristics of the proposed sensor are investigated and quantified. This paper is concluded in Section VI.

II. GEOMETRY DEFINITION AND PRINCIPLE OF OPERATION

The topology of the proposed sensor is shown in Fig. 1. It consists of a microstrip TL and a slot-fed cylindrical DR. The axis of the DR is aligned with the z axis and the feeding microstrip TL (with width w and length l) is adjusted to 50Ω . The port of the sensor is located at the beginning of the microstrip TL. The slot is etched on the ground plane beneath the DR which is constituted by a dielectric cylinder with the radius r_d , height h and ϵ_r dielectric constant. The DR bottom is fixed on the slot and the metallic ground plane. The dimensions of the slot are w_S and l_S . A small cylindrical pool with radius r_h and height h_h is embedded on top of the DR. This tank is used to allocate the liquid samples under test.

The dielectric cylindrical cavity resonator is conceptually similar to a circular waveguide. The total energy corresponding to the electric and magnetic fields are stored inside the cavity, affected by the dielectric permittivity of the DR. According to Fig. 2, the cylindrical cavity resonator can be considered as a parallel RLC . Accordingly, the reflection coefficient Γ_{in} can be obtained as

$$\Gamma_{in} = \frac{Z_{in} - Z_0}{Z_{in} + Z_0} \quad (1)$$

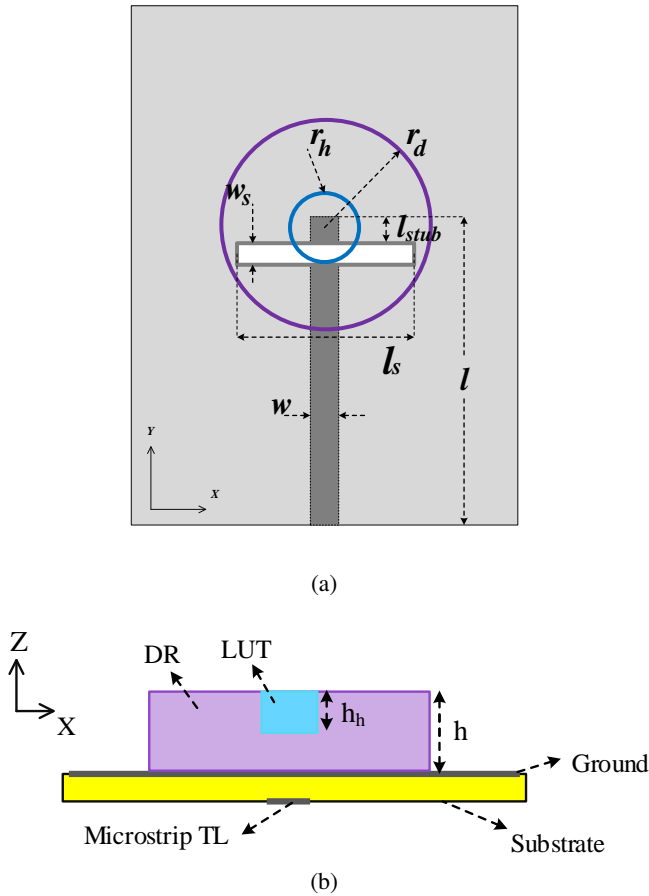


Fig. 1: DR Sensor (a) Front view, (b) Side view, with generic dimensions. The prototype's dimensions are reported in Table I.

where Z_{in} is the input impedance of the circuit and Z_0 is the intrinsic impedance of the port.

The resonant frequency of the DR can be defined as $\omega_0 = \frac{1}{\sqrt{LC_1}}$ and the unloaded Q-factor of DR can be interpreted as $Q_0 = \frac{\omega_0 L}{R}$. In critical-coupled condition wherein Z_0 equals to Z_{in} , the reflection coefficient approaches to zero. Through the implemented slot, the DR is coupled to the excited electromagnetic waves inside the microstrip host line. This is shown by the mutual coupling capacitor defined as C_m . By loading the DR to the TL, the resonant frequency of the loaded DR and subsequent loaded Q-factor are changed to

| Variable | Dimension [mm] |
|------------|----------------|
| r_d | 17 |
| h | 8 |
| r_h | 4 |
| h_h | 2.5 |
| w | 2.95 |
| l | 74 |
| w_s | 0.7 |
| l_s | 32 |
| l_{stub} | 6.65 |

TABLE I: Dimensions for the fabricated sensor. Variables are referred to Figure 1.

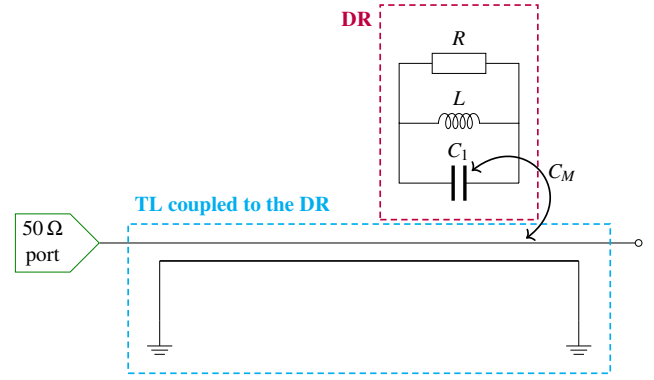


Fig. 2: Circuit model of the DR coupled to the microstrip transmission line.

$\omega = \frac{1}{\sqrt{L(C_1 + C_m)}}$ and $Q_L = \frac{\omega L}{(Z_{in} + R_{loss})}$ respectively. Here, R_{loss} is defined as lossy resistance corresponding to the TL and radiation dissipation.

The C_m capacitor is influenced by loading lossy liquids in the tank which is located on the sensitive area of the DR where the electric and magnetic fields confinement is strong. In particular, the total effective permittivity is perturbed when the hole is filled by the liquid sample. Therefore, every change in LUT leads to changes in ω and Q_L . Thus, this event makes changes in the Z_{in} and consequently the Γ_{in} changes. This reflection coefficient Γ_{in} is constantly measured. Therefore, the changes observed in this parameter depends on the LUT. In particular, the resonant frequency of sensor depends on the LUT and this is employed as the main sensing principle.

III. MODAL ANALYSIS AND PERTURBATION METHOD APPLIED TO THE SENSOR

For more insight into the DR sensor, the electromagnetic theory is applied to analyze the sensor's behaviour. The operation principle of the DR is based on the cavity electromagnetic model. By assuming the cavity resonator model, the analysis of the confined fields inside the DR can be conducted. It is provided by approximately considering the outer surfaces of the cavity as perfect magnetic conductors (PMC). In this approach, the eigen equations can be applied for the prediction of the DR resonant frequencies [24]. For practical proposes, pure TM_{nmp} and TE_{nmp} modes exist when the fields do not depend on the angular coordinate. Otherwise, the propagating mode is a combination of a TM and a TE mode, defined as Hybrid modes represented as HEM_{nmp} . The subscripts n , m and p are nomenclatures identifying the mode classification. The lowest of them is HEM_{110} [32]. As the radius of DR increases, the number of TE and TM modes and subsequently the hybrid modes number increases. The $HEM_{11\delta}$ mode, so-called dipole mode, is widely used in the DR structures in which δ is a non-integer value less than unity.

For small values of r_d , the field propagating outside of the DR can extend for a long distance whereas the fields for a large-radius DR are stronger confined closer to the DR. In this case, the phase constant β approaches to $\sqrt{\epsilon_r}\beta_0$ when the

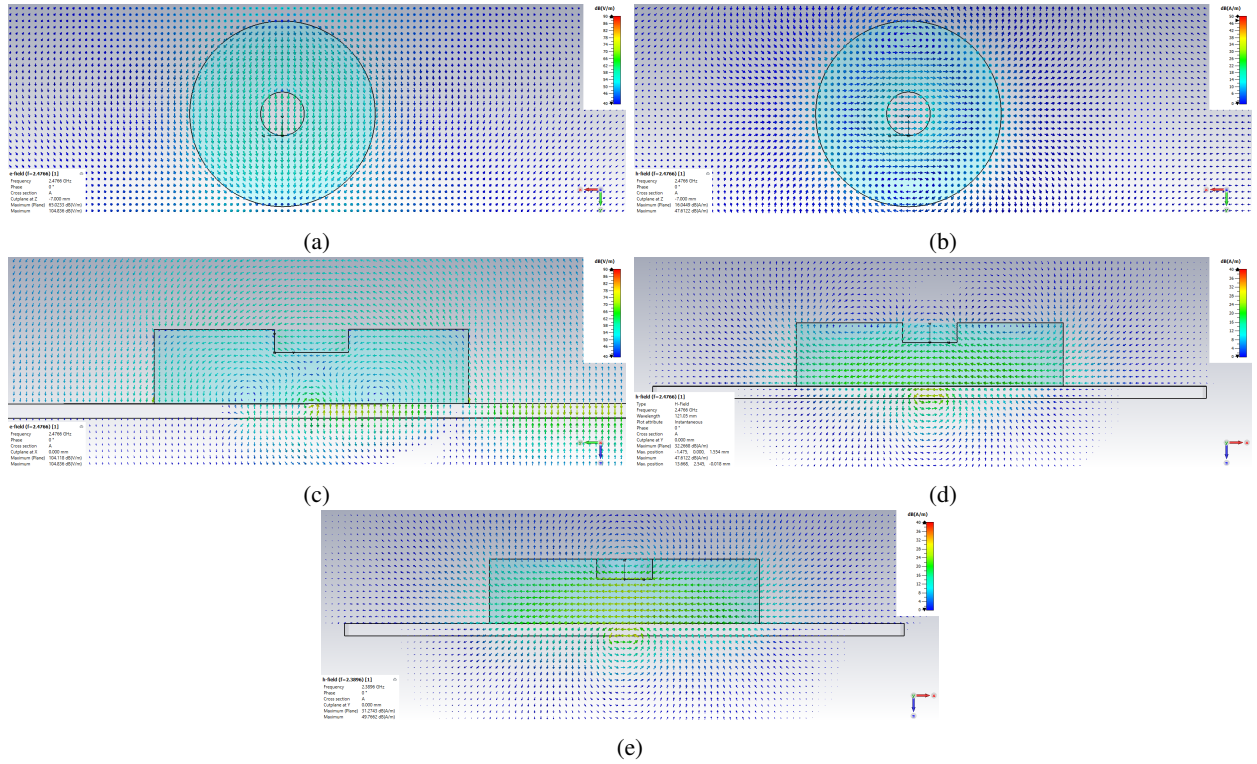


Fig. 3: Electric and magnetic field distributions of the fundamental mode (a) E field top view (unfilled sensor), (b) H field top view (unfilled sensor), (c) E field side view (unfilled sensor), (d) H field side view (unfilled sensor), (e) H field side view (sensor with water).

radius approaches to infinity considering β_0 the phase constant in free space. Therefore, the phase velocity is less than that of free space [33]. Unlike the fields equations for TM and TE modes which include both $\cos(m\phi)$ and $\sin(m\phi)$, the HEM modes have only either $\sin(m\phi)$ or $\cos(m\phi)$.

According to the previous explanation, HEM modes are excited inside the DR used as the base of the proposed sensor (Fig. 1). Specifically, the fundamental excited inside the DR is $HEM_{11\delta}$ [34], [35]. The resonant equation corresponding to the understudy $HEM_{11\delta}$, for the least value of δ , simplifies to:

$$(f_r)_{110} = \frac{c}{2r_d\pi\sqrt{\epsilon_r}} \times \left(1.71 + \frac{r_d}{h_d} + 1.578\left(\frac{r_d}{2h_d}\right)^2\right) \quad (2)$$

This resonant frequency corresponds to the unloaded equivalent cylindrical DR. As explained in Section II, when a small amount of liquid is inserted in the cavity, the resonant frequency of the resonator changes and an increase in the effective permittivity produces a decrease in the resonant frequency. On the other hand, the electromagnetic fields inside the DR remains almost unchanged. This can be also explained through the cavity perturbation technique. This technique is an accurate scheme which can be applied to analyse the change in the electromagnetic field distribution inside the cavity when the sample volume is very small to produce a negligible perturbation [36]. Here, the sample is considered as a thin-enough cylinder occupying the proposed hole which can satisfy the accuracy requirements for higher order modes. The fractional change in the resonant frequency due to the LUT

can be rewritten as follows (refer to the Appendix for more details):

$$\frac{\omega' - \omega}{\omega} = \frac{-\int_v \left(\Delta\epsilon |\vec{E}|^2 + \Delta\mu |\vec{H}|^2 \right) dv}{\int_v \left(\epsilon |\vec{E}|^2 + \mu |\vec{H}|^2 \right) dv} \quad (3)$$

where E and H are the electric and magnetic fields of the equivalent cylindrical DR (without any tank), ω and ω' are the resonant frequencies of the DR before and after placing LUT, respectively and Δ shows the variation in permittivity and permeability made by the LUT. According to Eq. 3, it can be clearly seen that by increasing the permeability and permittivity, there is a decrease in the resonant frequency, illustrating an increase in the stored energy in the resonant cavity. This is consistent with the operation principle presented in Section II. Furthermore, the resonant frequency variation depends on the location of the perturbation factor. In the other words, this fractional change in the resonant frequency is the result of interaction between electromagnetic fields inside of the DR and the LUT.

Finally, a full-wave simulation of the proposed sensor was performed by using CST Studio Suite. Figure 3 shows the electric and magnetic field distributions of the fundamental mode. The expected $HEM_{11\delta}$ mode is excited inside of the DR in which δ is a non integer less than unity. These field distributions are similar to the ones of a conventional cylindrical DR [37]. These demonstrates our previous theory as the fields inside the DR remain unchanged, but the fields

are confined in the pool when a sample is placed, as it can be seen in Fig. 3(e) compared to Fig. 3(d). This last interaction produces the desired frequency shift depending on the pool filling.

IV. MIXTURE PERMITTIVITY CHARACTERIZATION

The proposed DR sensor is utilized for characterizing different solutions of liquids. In particular, an ethanol-water solution was used to test the proposed sensor. In order to model the effective permittivity of binary mixtures, several formulations are used [38]. Maxwell Garnett model [39] with a simple appearance is widely used in vast-variety applications [38] which is written as

$$\epsilon_{eff} = \epsilon_{r_1} + 3|m|\epsilon_{r_1} \cdot \frac{\epsilon_{r_2} - \epsilon_{r_1}}{\epsilon_{r_2} + 2\epsilon_{r_1} - |m|(\epsilon_{r_2} - \epsilon_{r_1})} \quad (4)$$

wherein ϵ_{r_1} and ϵ_{r_2} are the dielectric constants of mixing two liquids with the mixing ratio of $(1-|m|)$ and $|m|$, respectively, while $|m| \leq 1$. It should be considered that for large dielectric constants, there is a very nonlinear function for effective permittivity. Before using this model, the permittivity of each liquid should be extracted separately. As the dielectric permittivity depends on the operation frequency, Debye- Γ relaxation model is used as a efficient tool for the permittivity extraction of ethanol at the desired frequency and $T = 25^\circ C$ (room temperature). The model equation is defined as

$$\epsilon = \epsilon_\infty + \frac{\epsilon_\infty - \epsilon_s}{1 + \frac{jf}{f_r}} - jf \times \Gamma \quad (5)$$

where ϵ_s and ϵ_∞ are defined as static permittivity and infinite permittivity respectively. Furthermore, f and f_r are corresponding to the desired frequency and resonance frequency respectively.

The resulting dielectric properties of the binary ethanol-water mixture are shown in Figure 4. There is a decrease of the relative permittivity and an increase of the losses when the percentage of ethanol increases. These results make sense because the relative permittivity and $\tan \delta$ of ethanol are much smaller and more higher than those of distilled water, respectively.

V. SIMULATION, MEASUREMENT AND DISCUSSION

A. Full-wave analysis and CST results

This section is devoted to the analysis of the performance of the proposed sensor. The sensor is tested with different ethanol-water solutions. First of all, the structure depicted in Figure 1 was optimized to obtain a sensor working in the ISM 2.45-GHz band, chosen because this is a freely available band, widely used in wireless applications, and with a handy availability of off-the-shelf-components. CST Studio Suite was used to perform the electromagnetic analysis of the sensor and the optimization of the DR and the coupling TL. The dielectric characteristics of the sensor and the final dimensions used for the simulation and fabrication are shown in Table II and Table I.

The results of the S_{11} parameter (reflection coefficient of the sensor, Γ_{in}) are shown in Figure 5. It can be seen how the

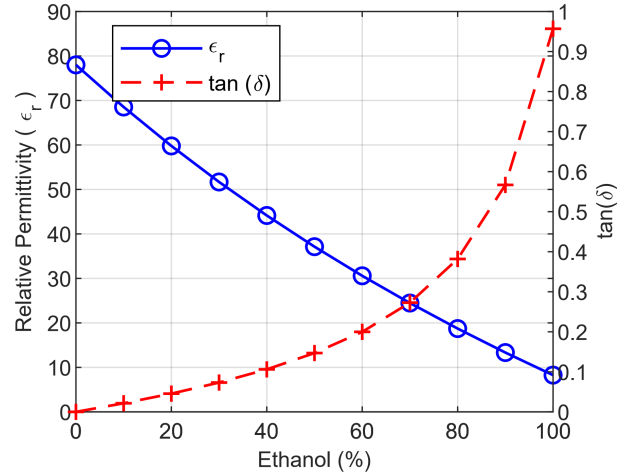


Fig. 4: Dielectric properties of the ethanol-water solution at 2.45 GHz.

| Parameter | TL Substrate (FR4) | DR (Zirconia) |
|----------------|--------------------|---------------|
| ϵ_r | 4.3 | 29.1 |
| $\tan(\delta)$ | 0.025 | 0.0019 |

TABLE II: Permittivity and $\tan(\delta)$ of the TL substrate and the DR used in the sensor.

original sensor without LUT is resonating at $2.48 GHz$ (dashed line). To emulate the loading with different ethanol-water concentrations, results from the permittivity model described in Section IV were used. Figure 5 also shows the behaviour of the sensor for the different solutions. As it could be expected, the resonance frequency increases as the ethanol concentration does, following the opposite trend of the dissolution's permittivity. This is, higher permittivities are related to lower concentrations, of ethanol which, in turns, leads to higher resonance frequencies. In conclusion, simulation results are in agreement with the desired operation principle of the sensor.

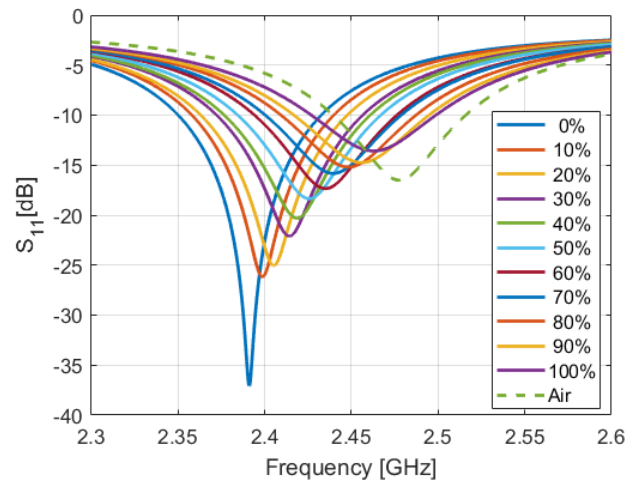


Fig. 5: S_{11} sensor response to different ethanol-water concentrations. Lines indicate the percentage of ethanol in water.

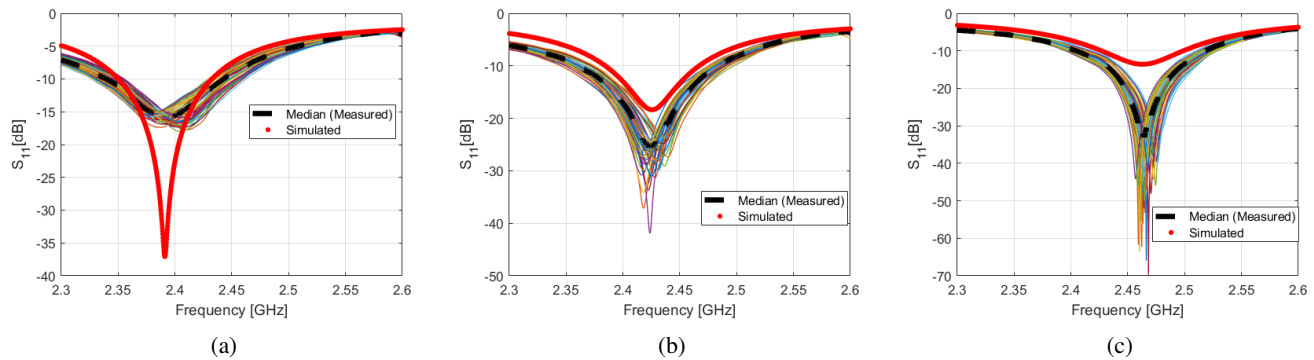


Fig. 6: Sensor response for different ethanol concentration. Simulated (red) versus measured (the thick dashed line is the average of the 61 measurements done for each concentration, that are drawn in thin colored lines). (a) 0% ethanol, (b) 50% ethanol, (c) 100% ethanol.

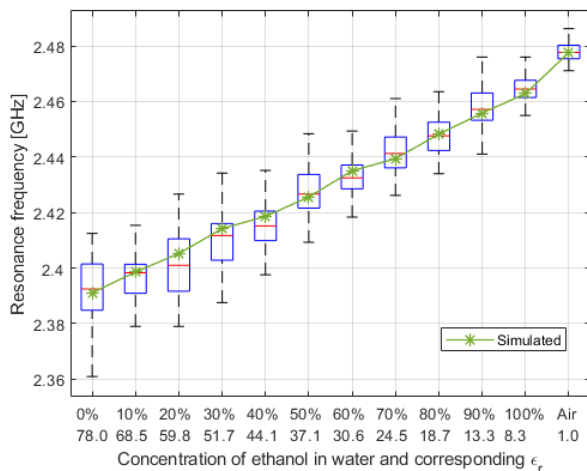


Fig. 7: Statistics of the resonance frequency as a function of the ethanol concentration. Boxplots are for measured data (average and standard variation over 61 experiments per concentration) while the line is for the simulated sensor.

B. Measurements and discussion

To evaluate the accuracy of the design outside of a simulation environment, the sensor depicted in Figure 1 has been fabricated and tested in a laboratory environment. A picture of the prototype can be seen in Fig. 8. The sensor has been fabricated by CarboSystem [40] and the base PCB by Eurocircuits [41] using standard processes, which helps in maintaining the cost of the sensor reasonably low.

Measurements referred in the following are done using an Anritsu MS46122B Vector Network Analyzer (VNA) to extract the S_{11} parameter of the sensor in the working band when placing ethanol/water concentrations in the range of 0% to 100% (taking steps of 10%) and without any LUT (air). The final sensor will be fitted in an *ad-hoc* electronic transceiver similar to the one presented in [42].

To evaluate the design versus the simulation a series of 61 measurements per concentration, summing up to a total of 732 measurements (from 0% to 100% concentration and including the air), cleaning the sensor between tests with distilled water



Fig. 8: Picture of the manufactured prototype.

and drying it with a microfiber cloth. All the measurements were made at laboratory average temperature, that is, between 20 and 25 degree Celsius, to remove this variable from the study.

Figure 6 shows a comparison of the S_{11} parameter for the simulated and fabricated sensor. Measurements on the fabricated sensor are done using different concentrations of ethanol and water. Figure 6(a), (b) and (c) shows the behaviour with distilled water (i.e. 0% ethanol), 50% of ethanol in water and 100% ethanol, respectively. Figures show colored lines with the different measurements taken, on top of them there is a black-dashed line indicating the median curve and a red-dotted line with the simulation result, for comparison.

It is worth to notice that, although the resonant frequency shifts and is different from the nominal frequency of 2.4 GHz, the changes are relatively tiny; using (4) and (5) the maximum permittivity variation due to the frequency shift can be assessed as a mere 0.3 in absolute value. This implies that the change in resonance frequency is fundamentally due the percentage change in the LUT, as expected.

As it can be seen, although there are some variations in the measurement (due to the sensitivity of the DR and the possible differences in LUT quantities applied), the overall trend is consistent. In addition to this, the position of the resonance in the simulated and median curve is in good agreement.

There exist a small discrepancy in the depth of the resonance, which the authors point to a mismatch in the $\tan(\delta)$ value used in the simulation and the actual value for the DR. Authors attribute this misalignment to the measurement setup.

To provide more detail about the repeatability of the measurements, Figure 7 shows a boxplot representation of the position resonance frequency for different concentrations. It can be seen how the statistics of the measurements are in good alignment with the simulated results, as the median measured values (red line inside the box) are very similar to the simulated results (green line). This same figure shows a consistent trend in the resonance frequency change as a function of the concentration for both measurements and simulations.

With respect to the sensitivity of the DR sensor, looking at the slope of the line in Figure 7, it can be approximated to 718kHz per percentage of ethanol in water.

VI. CONCLUSION

This paper presents a new technology to develop passive liquid sensors in the RF and microwave regime. The sensor itself is based on a cylindrical DR fed through a slot-coupled microstrip TL. The DR contains a small pool in order to allocate the LUT. The operation principle is as follows: the resonant frequency of the sensor depends on the electric permittivity of the LUT. This has been demonstrated by using an equivalent circuit approach and modal analysis. The cavity perturbation technique was used to study the impact of the LUT on the resonant frequency and modal distribution. Moreover, full-wave simulations were performed to check this theory. All the theory and simulations are consistent with the operation principle. Thus, the fundamental mode of the sensor similar to the $HEM_{11\delta}$ fundamental mode of a cylindrical DR but the electromagnetic fields interact with the LUT in the pool. This produces that the resonant frequency depends on the permittivity of the LUT. The proposed technology was tested with a complete set of ethanol-water solutions. A comprehensive method to characterize the mixture set is also presented in this work. This was used to simulate the performance of the sensor technology before manufacturing any prototype.

A prototype working in the low-GHz regime is designed, manufactured and measured. This prototype was optimized to work in the 2.45 GHz ISM band. Thus, this can be easily integrated with commercial electronics. Furthermore, up to the authors' knowledge, it is the first DR sensor working in the low-GHz band. The use of DR technology has some benefits over other electromagnetic sensors like higher Q factor and lower losses, leading to higher sensitivity, and higher temperature stability. The volume of the liquid samples for the proposed prototype is smaller than $0.13\ \mu\text{l}$. Hence, this is valid to sense small volumes of samples like biological measurements and some industrial applications like food or chemical industry such as oil characterization [43]. On the other hand, the complexity of the device is much reduced compared to others, like micro-fluidic devices. The dimensions are moderate and the cost is low when produced at high scale. As commented before, the sensor is passive and no batteries are needed. All these characteristics make this sensor a good candidate for sensing small-volume liquid samples in mass applications.

Finally, the manufactured prototype was tested in the laboratory with the ethanol-water set. The results matched well with simulations and showed good repeatability. The resonance frequency (minimum) in the reflection coefficient of the sensor was used as the sensing output. The sensitivity of the prototype is $718\ \text{kHz}$ per percentage of ethanol in water. The frequency of the minimum might not be the ideal detection mechanism but a combination of this approach and some pattern recognition in the reflection coefficient curve. However, this would be out of the scope of this paper but it seems a promising starting point for future works.

Aside from this discussion, the common approaches for dielectric spectroscopy need various bulky and expensive complex measurement setup such as, for example, a VNA connected to the sensor part for the frequency response extraction. Due to the VNA complexity, it cannot be a suitable spectroscopy system for a handheld and on-board sensing device. The sensor can be integrated with the electronic elements to be feasible as a portable device; the phase variations caused by the MUT/LUT can be detected by different output power or output voltages in an interferometry-based configurations. In a different approach, the electronic parts can also be integrated with a signal transmitter and a receiver consisting of a detector such as we have applied in other sensing structure [42]. That will be the matter for further research; this work just focuses on the DR sensing functionality.

APPENDIX

By considering E and H as the electric and magnetic fields of the original DR (without any hole) and E' , H' as the perturbed electromagnetic fields, respectively, the Maxwell equations are satisfying

$$\vec{\nabla} \times \vec{E} = -j\omega\mu\vec{H} \quad (\text{A.6})$$

and

$$\vec{\nabla} \times \vec{H} = j\omega\varepsilon\vec{E} \quad (\text{A.7})$$

When the material filling a small part of the cavity resonator the Maxwell curl equations can be written as:

$$\vec{\nabla} \times \vec{E}' = -j\omega'(\mu + \Delta\mu)\vec{H}' \quad (\text{A.8})$$

and

$$\vec{\nabla} \times \vec{H}' = j\omega'(\varepsilon + \Delta\varepsilon)\vec{E}' \quad (\text{A.9})$$

Wherein the ω and ω' are the resonant frequency of original and perturbed one respectively. The change in the permittivity and permeability are respectively noted as $\Delta\varepsilon$ and $\Delta\mu$. By conjugating the Equation A.6 and then multiplying by \vec{H}' and similarly, by conjugating the Equation A.9 and then multiplying by \vec{E}^* , we have:

$$\vec{H}' \cdot \vec{\nabla} \times \vec{E}^* = -j\omega'\mu\vec{H}' \cdot \vec{H}^* \quad (\text{A.10})$$

and

$$\vec{E}^* \cdot \vec{\nabla} \times \vec{H}' = j\omega'(\varepsilon + \Delta\varepsilon)\vec{E}^* \cdot \vec{E}' \quad (\text{A.11})$$

By subtracting these two equations according to the vector identity equation of $(\vec{\nabla}(\vec{A} \times \vec{B})) = \vec{B} \cdot \vec{\nabla}\vec{A} - \vec{A} \cdot \vec{\nabla}\vec{B}$, we have:

$$\vec{\nabla} \cdot (\vec{E}^* \times \vec{H}') = j\omega(\mu)\vec{H}' \cdot \vec{H}^* - j\omega'(\varepsilon + \Delta\varepsilon)\vec{E}^* \cdot \vec{E}' \quad (\text{A.12})$$

Similarly, this procedure should be applied to the eq. A.7 by multiplying E' and H^* which gives:

$$\vec{\nabla} \cdot (\vec{E}' \times \vec{H}^*) = -j\omega'(\mu + \Delta\mu)\vec{H}^* \cdot \vec{H}' + j\omega\varepsilon\vec{E}^* \cdot \vec{E}' \quad (\text{A.13})$$

By adding the last two equations, and using the divergence theorem, and defining the integral over the resonator volume, the following equation is achieved as:

$$\int_V \vec{\nabla} \cdot (\vec{E}' \times \vec{H}^* + \vec{E}^* \times \vec{H}') \cdot dv = \int_S (\vec{E}' \times \vec{H}^* + \vec{E}^* \times \vec{H}') \cdot ds = 0 \quad (\text{A.14})$$

And after rearrangement it gives:

$$j \int_V [\omega\varepsilon - \omega'(\varepsilon + \Delta\varepsilon)](\vec{E}^* \cdot \vec{E}') + [\omega\mu - \omega'(\mu + \Delta\mu)]\vec{H}^* \cdot \vec{H}' dv = 0 \quad (\text{A.15})$$

Based on image theory, the sum of tangential electric fields on the ground plane are zero, i.e., $\hat{n} \times \vec{E}' = 0$. According to the perturbation theory, it is expected that the electromagnetic fields are not greatly different from unperturbed ones when $\Delta\varepsilon$ and $\Delta\mu$ are small and the material under test is concentrated in a partially small volume. This approximation can be follows by assuming E'/H' equals E/H respectively, as the E' and H' fields are practically unknown. Consequently, the fractional change in resonant frequency is obtained as follows:

$$\frac{\omega' - \omega}{\omega} = \frac{-\int_V (\Delta\varepsilon |\vec{E}|^2 + \Delta\mu |\vec{H}|^2) dv}{\int_V (\varepsilon |\vec{E}|^2 + \mu |\vec{H}|^2) dv} \quad (\text{A.16})$$

ACKNOWLEDGMENT

This work has been funded by ‘‘IIT Strategic PhD Research Grants’’ and ‘‘Proyectos de Investigaci3n Propia’’ programs from Universidad Pontificia Comillas.

REFERENCES

- [1] G. Maenhout, T. Markovic, I. Ocket, and B. Nauwelaers, ‘‘Complementary split-ring resonator with improved dielectric spatial resolution,’’ *IEEE Sensors Journal*, vol. 21, no. 4, pp. 4543–4552, 2021.
- [2] P. Velez, J. Munoz-Enano, K. Grenier, J. Mata-Contreras, D. Dubuc, and F. Martin, ‘‘Split Ring Resonator-Based Microwave Fluidic Sensors for Electrolyte Concentration Measurements,’’ *IEEE Sensors Journal*, vol. 19, pp. 2562–2569, apr 2019.
- [3] C. L. Yang, C. S. Lee, K. W. Chen, and K. Z. Chen, ‘‘Noncontact measurement of complex permittivity and thickness by using planar resonators,’’ *IEEE Transactions on Microwave Theory and Techniques*, vol. 64, pp. 247–257, jan 2016.
- [4] A. Ebrahimi, J. Scott, and K. Ghorbani, ‘‘Ultrahigh-Sensitivity Microwave Sensor for Microfluidic Complex Permittivity Measurement,’’ *IEEE Transactions on Microwave Theory and Techniques*, vol. 67, pp. 4269–4277, aug 2019.
- [5] L. Su, X. Huang, W. Guo, and H. Wu, ‘‘A flexible microwave sensor based on complementary spiral resonator for material dielectric characterization,’’ *IEEE Sensors Journal*, vol. 20, no. 4, pp. 1893–1903, 2020.
- [6] A. M. Albishi, M. K. E. Badawe, V. Nayyeri, and O. M. Ramahi, ‘‘Enhancing the sensitivity of dielectric sensors with multiple coupled complementary split-ring resonators,’’ *IEEE Transactions on Microwave Theory and Techniques*, vol. 68, no. 10, pp. 4340–4347, 2020.
- [7] A. Javed, A. Arif, M. Zubair, M. Q. Mehmood, and K. Riaz, ‘‘A low-cost multiple complementary split-ring resonator-based microwave sensor for contactless dielectric characterization of liquids,’’ *IEEE Sensors Journal*, vol. 20, no. 19, pp. 11326–11334, 2020.
- [8] A. E. Omer, G. Shaker, S. Safavi-Naeini, K. Ngo, R. M. Shubair, G. Alqui3, F. Deshours, and H. Kokabi, ‘‘Multiple-cell microfluidic dielectric resonator for liquid sensing applications,’’ *IEEE Sensors Journal*, vol. 21, no. 5, pp. 6094–6104, 2021.
- [9] G. Maenhout, T. Markovic, I. Ocket, and B. Nauwelaers, ‘‘Complementary split-ring resonator with improved dielectric spatial resolution,’’ *IEEE Sensors Journal*, vol. 21, no. 4, pp. 4543–4552, 2021.
- [10] G. Galindo-Romera, F. Javier Herraiz-Mart3nez, M. Gil, J. J. Mart3nez-Mart3nez, and D. Segovia-Vargas, ‘‘Submersible Printed Split-Ring Resonator-Based Sensor for Thin-Film Detection and Permittivity Characterization,’’ *IEEE Sensors Journal*, vol. 16, pp. 3587–3596, may 2016.
- [11] M. Abdolrazzaghi, M. Daneshmand, and A. K. Iyer, ‘‘Strongly Enhanced Sensitivity in Planar Microwave Sensors Based on Metamaterial Coupling,’’ *IEEE Transactions on Microwave Theory and Techniques*, vol. 66, pp. 1843–1855, apr 2018.
- [12] E. Reyes-Vera, G. Acevedo-Osorio, M. Arias-Correa, and D. E. Senior, ‘‘A submersible printed sensor based on a monopole-coupled split ring resonator for permittivity characterization,’’ *Sensors (Switzerland)*, vol. 19, apr 2019.
- [13] M. G. Mayani, F. J. Herraiz Mart3nez, J. Matanza Domingo, and R. Giannetti, ‘‘Resonator-based microwave metamaterial sensors for instrumentation: Survey, classification and performance comparison,’’ *IEEE Transactions on Instrumentation and Measurement*, pp. 1–1, 2020.
- [14] P. Velez, L. Su, K. Grenier, J. Mata-Contreras, D. Dubuc, and F. Martin, ‘‘Microwave Microfluidic Sensor Based on a Microstrip Splitter/Combiner Configuration and Split Ring Resonators (SRRs) for Dielectric Characterization of Liquids,’’ *IEEE Sensors Journal*, vol. 17, pp. 6589–6598, oct 2017.
- [15] A. Salim, S. H. Kim, J. Y. Park, and S. Lim, ‘‘Microfluidic Biosensor Based on Microwave Substrate-Integrated Waveguide Cavity Resonator,’’ *Journal of Sensors*, vol. 2018, 2018.
- [16] A. A. Mohd Bahar, Z. Zakaria, M. K. Md. Arshad, A. A. Isa, Y. Dasril, and R. A. Alahnomi, ‘‘Real Time Microwave Biochemical Sensor Based on Circular SIW Approach for Aqueous Dielectric Detection,’’ *Scientific Reports*, vol. 9, no. 1, pp. 1–12, 2019.
- [17] D. Sievenpiper, L. Zhang, R. F. Jimenez Broas, N. G. Alex3polous, and E. Yablonovitch, ‘‘High-impedance electromagnetic surfaces with a forbidden frequency band,’’ *IEEE Transactions on Microwave Theory and Techniques*, vol. 47, no. 11, pp. 2059–2074, 1999.
- [18] A. Ernst, W. Streule, N. Schmitt, R. Zengerle, and P. Koltay, ‘‘A capacitive sensor for non-contact nanoliter droplet detection,’’ *Sensors and Actuators A: Physical*, vol. 153, no. 1, pp. 57–63, 2009.
- [19] Z. H. Zargar and T. Islam, ‘‘A novel cross-capacitive sensor for noncontact microdroplet detection,’’ *IEEE Transactions on Industrial Electronics*, vol. 66, no. 6, pp. 4759–4766, 2019.
- [20] H. Wei and A. A. Kishk, ‘‘Compact dielectric resonator antenna array for microwave breast cancer detection,’’ *2007 IEEE Region 5 Technical Conference, TPS*, pp. 9–12, 2007.
- [21] W. Huang and A. A. Kishk, ‘‘Compact dielectric resonator antenna for microwave breast cancer detection,’’ *IET Microwaves, Antennas and Propagation*, vol. 3, no. 4, pp. 638–644, 2009.
- [22] M. K. Saleem, M. Abdel-Rahman, M. Alkanhal, and A. Sebak, ‘‘A cylindrical dielectric resonator antenna-coupled sensor configuration for 94 GHz detection,’’ *International Journal of Antennas and Propagation*, vol. 2014, 2014.
- [23] S. K. K. Dash, T. Khan, and B. K. Kanaujia, ‘‘Circularly Polarized Dual Facet Spiral Fed Compact Triangular Dielectric Resonator Antenna for Sensing Applications,’’ *IEEE Sensors Letters*, vol. 2, no. 1, pp. 1–4, 2018.
- [24] D. Kajfez and P. Guillon, *Dielectric Resonators*. Artech House microwave library, Noble Publishing Corporation, 1998.
- [25] S. Sabrin, S. Kharkovsky, and R. Salama, ‘‘Dielectric resonator antenna integrated sensors for characterization of concrete,’’ *Proceedings of the International Conference on Sensing Technology, ICST*, vol. 2017-December, pp. 1–6, 2018.
- [26] M. Chauhan, A. K. Pandey, and B. Mukherjee, ‘‘A Novel Compact Cylindrical Dielectric Resonator Antenna for Wireless Sensor Network Application,’’ *IEEE Sensors Letters*, vol. 2, no. 2, pp. 1–4, 2018.
- [27] A. Iqbal, A. Smida, O. A. Saraereh, Q. H. Alsafasfeh, N. K. Mallat, and B. M. Lee, ‘‘Cylindrical dielectric resonator antenna-based sensors for liquid chemical detection,’’ *Sensors (Switzerland)*, vol. 19, no. 5, pp. 2–10, 2019.
- [28] I. Ali, M. H. Jamaluddin, A. Gaya, and H. A. Rahim, ‘‘A dielectric resonator antenna with enhanced gain and bandwidth for 5G applications,’’ *Sensors (Switzerland)*, vol. 20, no. 3, pp. 1–12, 2020.
- [29] K. W. Leung, ‘‘Development of Dielectric Resonator Antenna (DRA),’’ 2012.

- [30] A. Javed, A. Arif, M. Zubair, M. Q. Mehmood, and K. Riaz, "A low-cost multiple complementary split-ring resonator-based microwave sensor for contactless dielectric characterization of liquids," *IEEE Sensors Journal*, vol. 20, no. 19, pp. 11326–11334, 2020.
- [31] C.-S. Lee, B. Bai, Q.-R. Song, Z.-Q. Wang, and G.-F. Li, "Open complementary split-ring resonator sensor for dropping-based liquid dielectric characterization," *IEEE Sensors Journal*, vol. 19, no. 24, pp. 11880–11890, 2019.
- [32] D. Kajfez and A. A. Kishk, "Dielectric Resonator Antenna - Possible Candidate for Adaptive Antenna Arrays," 2002.
- [33] Balanis.C.A, *Antenna Theory Analysis and Design*. Wiley & Sons Inc, 1997.
- [34] A. A. Kishk, A. Ittipiboon, Y. M. M. Antar, and M. Cuhaci, "Slot excitation of the dielectric disk radiator," *IEEE Transactions on Antennas and Propagation*, vol. 43, no. 2, pp. 198–201, 1995.
- [35] A. K. Ojha, R. Jain, and P. Kumar AV, "Magnetic quadrupole mode excitation of a cylindrical dielectric resonator antenna using planar feed," *Microwave and Optical Technology Letters*, vol. 62, no. 1, pp. 484–490, 2020.
- [36] H. Gajera, D. Guha, and C. Kumar, "New Technique of Dielectric Perturbation in Dielectric Resonator Antenna to Control the Higher Mode Leading to Reduced Cross-Polar Radiations," *IEEE Antennas and Wireless Propagation Letters*, vol. 16, pp. 445–448, 2017.
- [37] D. Kajfez, A. W. Glisson, and J. James, "Computed modal field distributions for isolated dielectric resonators," *IEEE Transactions on Microwave Theory and Techniques*, vol. 32, no. 12, pp. 1609–1616, 1984.
- [38] A. Sihvola, "Mixing Rules with Complex Dielectric Coefficients," *Sub-surface Sensing Technologies and Applications*, vol. 1, no. 4, pp. 393–415, 2000.
- [39] A. A. Helmy, S. Kabiri, M. M. Bajestan, and K. Entesari, "Complex permittivity detection of organic chemicals and mixtures using a 0.5–3-ghz miniaturized spectroscopy system," *IEEE Transactions on Microwave Theory and Techniques*, vol. 61, no. 12, pp. 4646–4659, 2013.
- [40] "CarboSystems." <https://carbosystem.com/en/>.
- [41] "Eurocircuits." <https://www.eurocircuits.com/>.
- [42] M. G. Mayani, F. J. Herraiz Martínez, J. Matanza Domingo, R. Giannetti, and C. Rodríguez-Morcillo García, "Dual-Band Metamaterial-inspired Microwave Sensor For Liquid Dielectric Spectroscopy," in *Proceedings of IEEE International Instrumentation & Measurement Technology Conference (I2MTC)*, (Glasgow, Scotland), IEEE International Instrumentation & Measurement Technology Conference (I2MTC), 2021.
- [43] N. Tiwari, S. Singh, D. Mondal, and M. Akhtar, "Novel design of multi band compact planar rf sensor for liquid testing," in *2018 3rd International Conference on Microwave and Photonics (ICMAP)*, pp. 1–2, IEEE, 2018.



Mahdieh Gholami Mayani was born in Iran, in 1985. She received her Master's degree in Electrical Engineering from Shahid Beheshti University of Tehran in 2016. She has carried out various research topics and she achieved the best-researcher award in 2018 at the Electrical Engineering department of the Shahid Beheshti University. She joined the Instituto de Investigaciones Tecnológica (IIT), Madrid, Spain in 2019 as a researcher in training. Her areas of interest are biosensors, microwave filters, metamaterials,

numerical electromagnetism, passive and active devices, and multi-conductor transmission lines.



Francisco Javier Herraiz-Martinez received the Engineer and Ph.D. degrees (both First Class Hons.) in Telecommunications from Universidad Carlos III de Madrid, Madrid, Spain, in 2006 and 2010, respectively. During his doctoral stage, he was a visiting researcher at EPFL (Switzerland) and the University of Birmingham (UK). He spent a year with CIMITEC at UAB (Universitat Autònoma de Barcelona) as a Post-Doctoral Researcher. He was a Visiting Lecturer at Universidad Carlos III between 2012 and 2017. In 2017 he joined ICAI (Engineering School) of Universidad Pontificia Comillas, where currently he is an Assistant Professor. His research interests include passive sensors and RFID systems, electromagnetic metamaterials, antennas and microwave circuits. Dr. Herraiz-Martinez received the Best Master Thesis Dissertation Award from COIT/AEIT in 2006. He was a recipient of the Spanish Education Ministry official grant for funding his doctoral research activity.



Javier Matanza Domingo received his degree in Telecommunications Engineering from the Polytechnic University of Valencia in 2008 and his doctorate from the Comillas Pontifical University in 2013. He currently divides his tasks working on research projects at the Technological Research Institute (IIT) and as Assistant Collaborating Professor within the Degree in Engineering in Telecommunication Technologies and Master in Telecommunication Engineering at ICAI. His areas of interest are power cable transmission technologies (PLC), communication network simulation, co-simulation, demand response, communications for medical monitoring, signal processing and sensors.



Romano Giannetti received his degree in Electronic Engineering from the University of Pisa in 1989 and the PhD in Electronic and Computer Engineering from the University of Padua in 1993. He was a researcher in Pisa University (Italy) from 1994 to 1998, and since then he stayed at the Universidad Pontificia Comillas de Madrid (ICAI-ICADE) where is now Full Professor. His research interests are in the field of measurement instrumentation and methodology. He worked on the realization of high portable

measurement systems, in support instrumentation for microelectronic technology, in non-invasive techniques for blood gas measurements and in low noise measurement system aimed to the characterization of non-linear materials and to the recording of bioelectrical signals. He is senior member of Measurement and Education societies of IEEE.